Electric Power Systems Research 135 (2016) 59–67

Contents lists available at ScienceDirect

Electric Power Systems Research

journal homepage: www.elsevier.com/locate/epsr

Stochastic assessment of the impact of photovoltaic distributed generation on the power quality indices of distribution networks

Elson N.M. Silva, Anselmo B. Rodrigues, Maria da Guia da Silva*

Electrical Engineering Department, UFMA, São Luís, MA 65080-805, Brazil

ARTICLE INFO

Article history:
Received 20 October 2015
Received in revised form 3 March 2016
Accepted 4 March 2016
Available online 16 March 2016

Keywords:
Distributed power generation
Monte Carlo methods
Photovoltaic systems
Power distribution
Power quality
Time series analysis

ABSTRACT

This paper aims to assess the impact of photovoltaic distributed generation (PVDG) connection on the power quality indices (PQI) of distribution networks, such as: long term voltage variations (voltage conformity issues) and voltage unbalance. The stochastic nature of PVDG and loads were considered in the study using probabilistic techniques. The impact of PVDG on the number of tap changes of the voltage regulators was investigated. The tests results in a real life large scale distribution network demonstrated that the PVDG can cause around 31% of improvements in the voltage conformity indices. This impact is less beneficial than the one associated with the connection of conventional distributed generation due to the variability in the primary energy resource. Furthermore, it was demonstrated that the connection of PVDG increases the lifespan of the voltage regulators as a result of a reduction about 20% in the number of tap changes.

1. Introduction

One of the most prominent renewable distributed generation (DG) is the solar based on photovoltaic conversion. In Brazil, the photovoltaic DG (PVDG) has been stimulated due to the high levels of solar irradiation thanks to favorable geographical conditions and reduction in the photovoltaic panel's costs.

The technical assessment of PVDG installation in the distribution network must consider its impact on the performance indices associated with: resistive losses, feeder loading and power quality. Power quality disturbances may cause tripping or inadequate operation of customer's equipment. Furthermore, regulatory agencies establish penalties for distribution utilities that do not meet power quality targets. Consequently, several studies have been carried out to assess the impact of PVDG in power quality indices, such as: voltage unbalance [1] and harmonics [2,3]. Other important power quality disturbance is the long-term voltage variations. Namely, deviations in the voltage RMS value, at the nominal frequency of the network, with durations greater than 1 min. In Brazil, the problems of power quality related to long-term voltage variations are denominated as voltage conformity problems [4]. The regulatory agencies [4] and international standards [5] define voltage conformity indices based on the cumulative duration associated with a nodal voltage. That is, the total duration, in percentage terms of the monitoring period, in which a nodal voltage has been outside of a specified interval.

The PVDG introduces uncertainties in the planning and operation of distribution networks due to large variations in its output power caused by the stochastic behavior of the solar irradiation. Several papers have proposed methodologies to model uncertainties associated with PVDG in the performance assessment of distribution networks [6–12]. In these references, the preferred approach to model uncertainties in PVDG is the probabilistic load flow (PLF). The PLF methods used for this purpose can be classified in accordance with the representation of the uncertainties in three categories:

(i) Non-Sequential [6,7]: the performance indices are evaluated for a single time interval, such as the peak load. Therefore, the temporal dependence in the uncertainties is ignored.
(ii) Pseudo-Stochastic [8–10]: the evaluation of the performance indices is carried out for a study period (daily or weekly). Usually, the study period is divided into intervals with durations from 1 s up to 1 h. This representation recognizes the temporal dependence of the uncertainties related to PVDG and load, but the serial correlation of the uncertainties among the time intervals is not completely represented. The most used techniques to solve the PLF in the pseudo-stochastic representation

* Corresponding author. Tel.: +55 98 32729227; fax: +55 98 3301 8241.
E-mail addresses: elson-ms@hotmail.com (E.N.M. Silva), anselmo@dee.ufma.br (A.B. Rodrigues), guia@dee.ufma.br (M. da Guia da Silva).

http://dx.doi.org/10.1016/j.epsr.2016.03.006
0378-7796/

are: the Monte Carlo Simulation (MCS) [8] and the analytical [9,10].

(iii) Stochastic [11,12]: in this representation the serial correlation in the uncertainties is accurately modeled using the time series theory. Due to the temporal correlation among the time intervals of the study period, the most suitable technique to solve the PLF problem in the stochastic representation is the MCS with sequential sampling.

Some algorithms used in the non-sequential and pseudo-stochastic representations to solve the PLF are based on elegant mathematical methods such as: Nataf Transformation and Latin Hypercube Sampling [6], Cornish–Fisher expansion [7,10] and Point-Estimate [9]. These algorithms have low computational cost regarding to the MCS because the probability distributions of the voltages are obtained using analytical formulas. However, these algorithms have limited practical application since they cannot estimate cumulative duration indices used in voltage conformity assessment. This limitation is due to the fact that the analytical solution of the PLF generates the probabilities distributions of the nodal voltages, but not a cumulative duration indices, since they are associated with a chronological test function of the nodal voltages. In other words, the cumulative duration indices are not directly associated with nodal voltages, but with the summation of the time intervals in which a nodal voltage stayed in a specified interval. This summation is dependent of the chronological state transition processes of the system due to the uncertainties in the stochastic behavior.

The stochastic representation is preferable with regarding to pseudo-stochastic and non-sequential representations due to its capacity to recognize serial correlation in the system uncertainties. However, this representation has a high computational cost due to the utilization of MCS to evaluate the performance indices. In spite of that, the stochastic representation is the only available option to evaluate indices associated with the cumulative duration of an event for a study period, such as the voltage conformity. Additionally, the regulatory agencies [4] and international standard [5] for electric energy supply establish targets for the cumulative duration indices related to long term voltage variations. For example, the EN 50160 [5] determines that the voltage magnitude in low and medium voltage distribution networks must stay in the range ±10% for 95% of the time in a week. The estimation of the risk in violating targets for voltage conformity indices requires the probability distributions for these indices. The stochastic representation is the only approach capable to generate these distributions. It is important to emphasize that the setting of a target for voltage conformity indices is well known, but there is no paper that has considered the impact of DG on the risk related to these targets. In this way, the stochastic representation can support distribution utilities planning engineers to identify the DG penetration level that has acceptable risk of violating the target for voltage conformity indices. Additionally, it is possible to estimate the expected loss of revenue of a distribution utility due to penalties as a result of poor voltage conformity indices.

Other important issue related to technical impact of the DG connection is the number of tap changes of voltage regulators. Voltage regulators are installed in conventional distribution networks to maintain the control node voltage in a specified range through the tap changes. When a DG (conventional or photovoltaic) is connected to distribution network the number of tap changes can increase or decrease due to the factors: operation mode of the conventional DG (peak shaving or base load), intermittence of the primary energy resource (wind speed or solar irradiation) and DG failures. The excessive number of tap changes can cause lifetime loss of the voltage regulator due to the presence of impurities caused by arcs and due to the wear owing to movement of mechanical parts [13]. Furthermore, the effects of PVDG integration on the operation of var/volt control devices are currently considered as a great challenge due to the large penetration potential of PVDG in distribution networks [14–16]. Therefore, it is worth to consider the number of tap changes in the technical analysis of DG connection. In the sense to provide more realistic and useful results, it is necessary that the predictive model include uncertainties associated with: solar irradiation, temperature and load fluctuations.

The proposal of this paper is to assess the impact of PVDG insertion on the voltage conformity and unbalance indices. This assessment is carried out using probabilistic approaches to model the stochastic system behavior related to load fluctuations and solar irradiation. Furthermore, the proposed model considered uncertainties associated with temperature variations and DG availability. The selected probabilistic approach to estimate the power quality indices is the PLF with stochastic representation, based on the Quasi-Sequential MCS [17]. The nodal voltages of the system for each scenario generated by the Quasi-Sequential MCS are calculated using a load flow algorithm based on phase-coordinates model [18]. The sample of the system scenarios was used to: compute cumulative duration indices related to voltage conformity, estimate the risks of violating power quality targets and to obtain the chronological variations in the voltage unbalance index. The proposed methodology was tested in a real life primary distribution feeder with 1560 nodes. The results demonstrate that the PVDG connection has a significant impact on the PQI, but its effect is less beneficial than the one associated with conventional DG. Additionally, the impact of DG connection on the number of tap changes of the voltage regulators was investigated.

2. Deterministic and probabilistic models

2.1. Load flow algorithm based on phase-coordinates model

To estimate PQI in a distribution network it is necessary to determine the nodal voltages of the network. These voltages must be calculated considering the unbalanced nature of the power distribution network. This issue can be taken into account using phase-coordinate models for the components [18]. It is possible to combine these models with backward/forward sweep techniques to obtain fast and accurate load flow algorithms for radial distribution networks. In this paper, the backward/forward sweep load flow proposed in [18] is used to evaluate the nodal voltages for each time interval of a system scenario generated by the Quasi-Sequential MCS.

2.2. Time series models for temperature, solar radiation and load

In order to evaluate the cumulative duration indices associated with voltage conformity, it is required to model the temporal dependence of the temperature, solar irradiance and feeder load. In this paper, the autoregressive moving average (ARMA) and Fourier models were used to model these time series. The generic form of the time series model used to represent the stochastic behavior of the temperature and solar irradiation is given by (1):

$$Z_t = S_t + x_t \tag{1}$$

where $S_t = b_0 + \sum_{h=1}^{N_h}[a_h \sin(\omega_h t) + b_h \cos(\omega_h t)]$ is the seasonal component modeled using the Fourier harmonic model. N_h is the number of harmonics. a_h and b_h are the coefficients related to the harmonic component h. ω_h is the frequency associated with the harmonic component h. x_t is the residual which contains a white noise w_t (with zero mean and constant variance σ^2) and perhaps other additional signals.

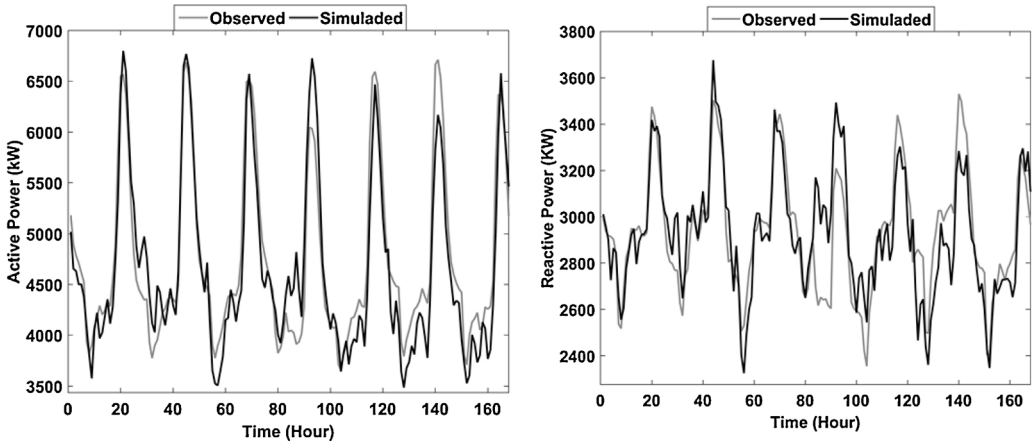

Fig. 1. Observed and simulated active (left) and reactive (right) load curves.

Table 1
Load curve parameters.

Parameter	Value
Peak load	6986 kW
Mean load	4759.7 kW
Load factor	68.1%
Mean power factor	0.8455

The residuals are represented by the ARMA(p,q) model defined in (2):

$$x_t = \phi_1 x_{t-1} + \cdots + \phi_p x_{t-p} + \theta_1 w_{t-1} + \cdots + \theta_q w_{t-q} + w_t \quad (2)$$

$\phi_1, \ldots, \phi_p$ are the parameters of the auto-regressive model with order p; $\theta_1, \ldots, \theta_q$ are the moving average parameters with order q.

The identification and estimation procedures of the models defined in (1) and (2) are explained in Ref. [19]. After the time series models have been obtained, they can be used to generate a sample of a simulated time series to the load, temperature and irradiance. Ref. [19] presents the algorithm used to produce the simulated time series from models (1) and (2).

The proposed methodology in this paper has been tested in a feeder of an Electricity Distribution Utility in the Northeast region in Brazil. Table 1 shows some parameters of the hourly active/reactive load curves of this feeder for January of 2009. That is, the total number of load levels is 744 (31×24).

The time series models for the load curves have been adjusted considering the historical load data for January 2009. In other words, there are about four weeks of observed time series for the load curve. This amount of data is sufficient to set up a model to carry out a weekly load forecasting [20]. The time series model for the load curve can be obtained using the same approaches used to derive the models related to irradiance and temperature. Table 2 shows the Fourier harmonic model for the active and reactive loads. Additionally, Eqs. (3) and (4) present the ARMA(4,3) and ARMA(4,4) models used to represent the active and reactive load residuals:

$$x_t^{watt} = -0.17x_{t-1}^{watt} + 0.0012x_{t-2}^{watt} + 0.227x_{t-3}^{watt} + 0.4997x_{t-4}^{watt} + 0.8674w_{t-1}^{watt} + 0.4119w_{t-2}^{watt} + 0.4328w_{t-3}^{watt} + w_t^{watt} \quad (3)$$

$$x_t^{var} = 0.4748x_{t-1}^{var} - 0.5715x_{t-2}^{var} + 0.9478x_{t-3}^{var} - 0.0838x_{t-4}^{var} + 0.2682w_{t-1}^{var} + 0.46729w_{t-2}^{var} - 0.3452w_{t-3}^{var} - 0.204w_{t-4}^{var} + w_t^{var} \quad (4)$$

where x_t^{watt} (x_t^{var}) is the forecasted value for the residuals time series related to active (reactive) load in the time t and w_t^{watt} (w_t^{var}) is the white noise associated with the active (reactive) load with variance 134.5206 kW (65.8276 kVAr).

The forecasted active and reactive loads for the feeder are allocated at the load points using a participation factor based on the rated power of the transformer in which the load is connected [18].

Fig. 1 shows the simulated and observed load curves for the test feeder in the third week of January 2009. From this figure, it can be concluded that the simulated time series for the active and reactive load curve are well fitted to their corresponding observed time series.

2.3. PVDG electrical modeling

The PVDG system is composed of photovoltaic (PV) arrays connected to an inverter DC/AC to deliver energy to the grid and/or customer's facilities. The active power generated by a PVDG is obtained from (5) [21]:

$$P_{AC} = \eta_{inv} \times \eta_m \times \eta_d \times P_{CC} \quad (5)$$

Table 2
Fourier harmonic model for the active and reactive loads.

Active load				Reactive load			
h	ω_h	a_h	b_h	h	ω_h	a_h	b_h
0	0	∄	4759.74	0	0	∄	2956.031
1	0.2617994	−547.9616	878.7723	1	0.2617994	−239.0911	186.4182
2	0.5235988	−408.8754	159.213	2	0.008445142	115.5776	34.99483
3	0.7853982	−283.0208	−253.1857	3	0.5235988	−78.69414	80.9676
4	0.008445142	169.3079	50.13978	4	0.7853982	−59.84728	−87.30002
5	1.308997	113.7094	53.78796	5	0.01689028	52.02907	27.92631
6	1.047198	−10.37443	−108.3027	6	0.1857931	32.02985	36.90315
∄	∄	∄	∄	7	1.308997	38.16747	21.67543

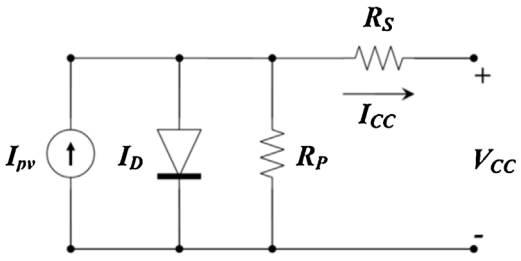

Fig. 2. Equivalent circuit for the PV module.

where P_{CC} is the DC power generated by the PV array; P_{AC} is the active power generated by the inverter for a given value of P_{CC}; η_{inv}, η_m and η_d are the constants used to consider the following effects: inverter efficiency, mismatch among the PV modules and dirt, respectively. The values of these constants are in accordance with [22]: $\eta_{inv} = 0.9$, $\eta_m = 0.97$ and $\eta_d = 0.96$. The P_{CC} value is calculated from (6) which in turn is obtained from the $I \times V$ curve of the PV modules:

$$P_{CC} = \max(V_{CC} \times I_{CC}) \tag{6}$$

where V_{CC} and I_{CC} are, respectively, the current and voltage generated by the PV array and max(*) is the Maximum Power Point Tracking (MPPT) function.

A PV array is composed of a series and parallel combination of several modules. The equivalent circuit is presented in Fig. 2 [23,24], where: R_S (R_P) is series (parallel) resistance; I_D is the diode current and I_{pv} is the current generated by the light incidence.

From the equivalent circuit in Fig. 2, the values of V_{CC} and I_{CC} for a PV array can be calculated from (7) [23,24]:

$$I_{CC} = I_{pv}N_{par} - I_0 N_{par}[\exp(\delta_1) - 1] - \delta_2 \tag{7}$$

where

$$\delta_1 = \frac{V_{CC} + R_s N_{ser}/N_{par} I_{CC}}{aV_t N_{ser}} \tag{8}$$

$$\delta_2 = \frac{V_{CC} + R_s N_{ser}/N_{par} I_{CC}}{R_p N_{ser}/N_{par}} \tag{9}$$

$$I_{pv} = (I_{pv,n} + K_I \Delta_T) G/G_n \tag{10}$$

$$I_0 = \frac{I_{pv,n} + K_I \Delta_T}{\exp[(V_{oc,n} + K_V \Delta_T)/aV_t] - 1} \tag{11}$$

N_{ser} is the number of modules in series; N_{par} is the number of strings of modules in parallel; I_0 is the reverse saturation current of the PV module; $V_t = N_S kT/q$ is the thermal voltage of a PV module composed of N_{ser} cells in series; q is the elementary charge of the electron ($1.60217646 \times 10^{-19}$); k is the Boltzman constant ($1.3806503 \times 10^{-23}$); T is the temperature of the p–n junction; $I_{pv,n}$ is the PV current, in amperes, generated in nominal conditions (temperature of 25 °C and solar irradiation of 1000 W/m^2); $\Delta_T = T - T_n$; T_n is the nominal temperature in Kelvin degrees; G is the incident radiation in the surface of the module in W/m^2; G_n is the nominal solar irradiation; K_I and K_V are the coefficients of current/temperature (A/K) and voltage/temperature (V/K), respectively.

2.4. PVDG reliability modeling

One kind of uncertainty which is usually ignored in studies related to technical assessment of PVDG connection is the reliability of the PVDG. Typical PVDG systems are composed of several components (strings, fuses, inverter, etc.) An individual failures of a component can lead to a total or partial loss of the power output. Consequently, the PVDG reliability can introduce more uncertainties in the estimation of the PQI of the distribution network. In this paper, the PVDG reliability is considered in the evaluation of the PQI using the model proposed in [25]. Based on this reference, the failure rate (λ_S), the unavailability (U_S) and the repair (r_S) time of a string composed of m PV modules in series are given by:

$$\lambda_S = \sum_{i=1}^{m} \lambda_{P,i} + \lambda_F \tag{12}$$

$$r_S = \left(\sum_{i=1}^{m} \lambda_{P,i} r_{P,i} + \lambda_F r_F \right) / \lambda_S \tag{13}$$

$$U_S = \lambda_S / (\lambda_S + 1/r_S) \tag{14}$$

where $\lambda_{P,i}$ ($r_{P,i}$) and λ_F (r_F) are the failure rates (repair times) of a PV module i and the fuse, respectively.

Consequently, the failure probabilities for an array composed of n identical strings connected in parallel is evaluated using the binomial distribution as:

$$P_r = C_{r,n} U_s^r (1 - U_s)^{n-r} \tag{15}$$

where P_r is the failure probability of r strings and the notation $C_{r,n}$ indicates the number of combinations of r items selected from n items.

In this way, the number of failed strings of a PVDG for a given state of a scenario generated by MCS can be obtained by sampling random numbers using a binomial distribution with input parameters: n, r and U_S. One parallel association of strings is connected to each phase through an inverter. Consequently, the power output of a phase is zero if the inverter is unavailable. In the MCS, the inverter state (up or down) is determined by sampling a uniform random number generator. If the uniform random number is smaller than the inverter unavailability, then the inverter is in the down state. Otherwise, the inverter is in the up state.

For the conventional DG, the state of sampling is simpler. Firstly, a uniform random number is generated. If this random number is smaller than the DG's FOR (Forced Outage Rate), then the DG is in down state. Otherwise, the DG is in up state.

3. Conceptual algorithm of the proposed methodology

According to the Section 1, the best alternative to assess the PVDG impact on PQI associated with cumulative durations is the PLF with stochastic representation. In this paper, the PLF with stochastic representation is solved through the Quasi-Sequential MCS [17].

The algorithm to estimate the power distribution PQI through the Quasi-Sequential MCS is exhibited in the flowchart of Fig. 3, where: NS^{max} is the maximum number of system scenario samples and NT is the number of time intervals in which the study period is divided (168 for a weekly load curve with load steps of 1 h).

The test functions for the PQI considered in this paper are defined below:

(i) Individual relative duration of the voltage conformity state S at the load point i ($IRD_{S,i}$)

$$IRD_{S,i}^k = \frac{100\%}{T} \sum_{t=1}^{NT} IRD_{S,i}^k(t) \tag{16}$$

(ii) Equivalent relative duration of the voltage conformity state S (ERD_S)

$$ERD_S^k = \left[\sum_{i=1}^{NL} IRD_{S,i}^k \right] / NL \tag{17}$$

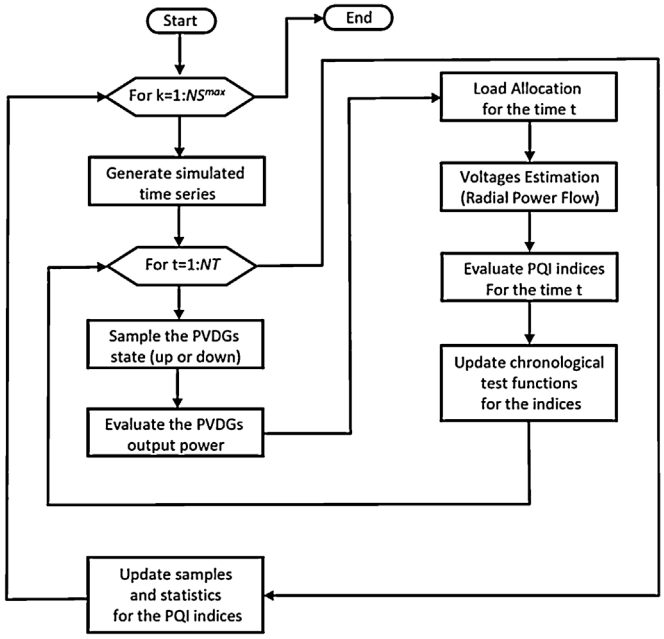

Fig. 3. Flowchart of the proposed algorithm.

(iii) Customer index with critical voltage (*CIC*)

$$CIC^k = 100\% \times \left[\sum_{i=1}^{NL} CIC_i^k\right] / NL \tag{18}$$

(iv) Voltage unbalance index for the time t ($VUI(t)$),

$$VUI^k(t) = \max\{\rho_i^k(t), \quad i = 1, \ldots, NL\} \tag{19}$$

where $S \in \{A, P, C\}$ is a subscript that identifies the voltage conformity states Adequate (A), Precarious (P) Critical (C) in accordance with the Brazilian regulation and with the EN 50160. The voltage ranges for the Brazilian regulation are defined in Table 3 [4]. In the EN 50160 there is only the adequate state in which the voltage range is [0.90, 1.10] pu. $IRD_{S,i}^k$ is the test function associated with the index $IRD_{S,i}$ for the system scenario k. T is the total duration of the study period. In this paper, $T = 168$ (7×24) h because the Brazilian regulation for power quality standards and the EN 50160 establish that the voltage conformity indices must be measured in a weekly period. $IRD_{S,i}^k(t)$ is a test function which is equal to one if the voltage at the load point i is in the voltage conformity state S for the time interval t. Otherwise, $IRD_{S,i}^k(t) = 0$. ERD_S^k is the test function associated with the index ERD_S for the system scenario k. NL is the number of load points. CIC^k is the test function associated with the index CIC for the system scenario k. CIC_i^k is the test function related to the index CIC at the load point i for the scenario k. This function is unitary if $IRD_{C,i}^k > 0$. Otherwise, it is equal to zero. $VUI^k(t)$ is the test function for the index $VUI(t)$ for the scenario k.

Table 3
Brazilian voltage conformity states voltage from 1 kV up to 69 kV.

Voltage conformity state	Voltage range (pu)
Adequate	[0.93, 1.05]
Precarious	[0.90, 0.93)
Critical	(−inf, 0.90) or (1.05, +inf)

$$\rho_i^k(t) = 100\% \sqrt{\frac{1 - \sqrt{3 - 6\beta_i^k(t)}}{1 + \sqrt{3 - 6\beta_i^k(t)}}} \tag{20}$$

$$\beta_i^k(t) = \frac{[V_{AB,i}^k(t)]^4 + [V_{BC,i}^k(t)]^4 + [V_{CA,i}^k(t)]^4}{\{[V_{AB,i}^k(t)]^2 + [V_{BC,i}^k(t)]^2 + [V_{CA,i}^k(t)]^2\}^2} \tag{21}$$

$V_{AB,i}^k(t)$, $V_{BC,i}^k(t)$ and $V_{CA,i}^k(t)$ are the line voltages between the phases AB, BC and CA, respectively, at the load point i for the time interval t of the scenario k.

The test functions associated with the voltage conformity indices for a load point i ($IRD_{A,i}$, $IRD_{P,i}$ and $IRD_{C,i}$) express the average cumulative duration in which the voltage at the load point i stayed in a voltage conformity state (adequate, precarious or critical). On the other hand the systemic (equivalent) voltage conformity indices (ERD_A, ERD_P and ERD_C) indicate the average cumulative duration of a voltage conformity state for each load point, that is, they are equivalent to the mean of the load point indices for a set of customers. The CIC index represents the percentage of customers in which the average cumulative duration of the critical state is not zero. Additionally, the $VUI(t)$ represents the maximum unbalance of voltage for a set of load points in the time t based on the voltage unbalance factor defined in [26]. Due to this, this index has temporal dependence. The PQIs defined in this paper are a comprehensive set of measures for the power quality assessment of PVDG integration to the grid because they are used by regulatory agencies and international standard to define power quality targets. Consequently, they are widely used by distribution utilities and can be easily interpreted by planning engineers involved in studies of technical impact with PVDG connection.

4. Tests results

4.1. DG siting and sizing

The proposed method in this paper has been tested in a real life primary feeder of a utility located in the Northwest of Brazil. The main characteristics of this feeder are presented in Table 4 [27].

The first step to assess the impact of DG connection on the PQI indices in the test system is to define the site and size of the DG. This definition was carried out minimizing the sum of the indices ERD_P and ERD_C. To solve this optimization problem, it was first defined 30% of the forecasted system peak load as the DG penetration level in the distribution network. Next, it was considered that the capacity of each DG is 750 kW. Consequently, the maximum number of DG units that must be allocated is equal to the penetration level divided by the capacity of each DG. In this way, the number of DG that will be allocated is: $0.30 \times 6986\,\text{kW}/750\,\text{kW} = 2.7944 \approx 3$, where 6986 kW is the forecasted system peak load.

All load points with $IRD_{C,i}$ greater than zero are set as candidate places for installing these three DG. For the forecasted peak load condition, there are 35 load points with $IRD_{C,i}$ greater

Table 4
Main characteristics of the test system.

Characteristic	Value
Number of nodes	1560
Number of fuses	119
Number of trunk sections	389
Number of lateral sections	1889
Number of transformers	148
Voltage class	13.8 kV
Total length	42.3926 km
Total number of customers	18,483

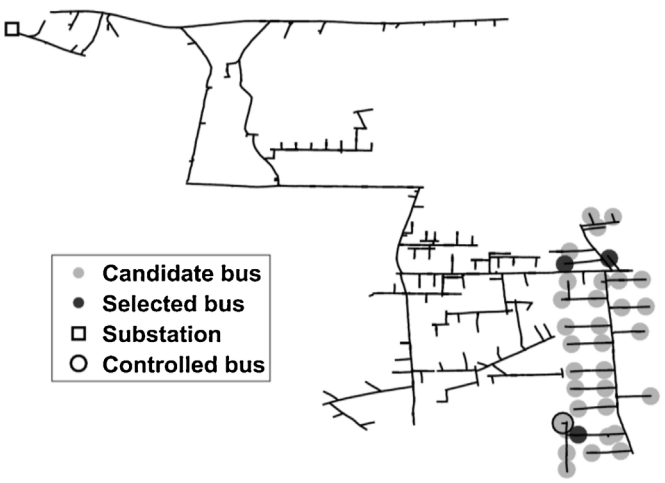

Fig. 4. DG placement in the test feeder.

than zero. Therefore, the number of candidate solutions is: $C_{0,35} + C_{1,35} + C_{2,35} + C_{3,35} = 7176$. It is not feasible to assess all the combinations associated with candidate solutions using an exact model for the electrical network and the load curve, since it is necessary to solve $24 \times 31 = 744$ power flow problems to estimate the voltage conformity indices for each candidate solution. To overcome this difficulty the following simplifications has been considered:

(i) the active and reactive load curves are clustered in 7 levels.
(ii) Positive sequence load were used instead of phase-coordinate model.

The optimal DG placement is determined by finding the DG combination that achieve the minimum value for the sum of the indices ERD_P and ERD_C in accordance with the conceptual algorithm:

(i) Select a site for the DG allocation from the candidate places;
(ii) Estimate the voltage conformity indices for the selected site using the simplified network model.
(iii) If the objective function of the selected site is smaller than the current optimal solution, then the selected site is considered as the new optimal solution.
(iv) Repeat the steps (i)–(iii) for all the combinations of sites for the DG allocation.

The candidate and selected places for the DG installation in the test feeder are presented in the GIS (Geographic Information System) one-line diagram of Fig. 4. From this figure, it can be observed that the DG was installed far from the substation. This result was expected once that the voltage drops at the load points far from the source are more severe. The DG placement procedure has the following constraints: (i) only one DG can be allocated in each candidate place; (ii) all the allocated DG has the same size; (iii) the maximum penetration level for the DG installation must be specified. If these constraints are not satisfied, then optimization algorithms must be used to solve the DG allocation procedure. The accuracy of the DG allocation procedure can be assessed evaluating the ERD_A index with the exact (phase-coordinate with original monthly load curve) and approximated (positive sequence with load curve clustering) models before and after the DG allocation. The values of the ERD_A and the relative errors are presented in Table 5. The relative errors associated with the ERD_A index were evaluated regarding to the exact model. From Table 5, it can be concluded that the approximated model can estimate the voltage conformity index with acceptable precision because the relative errors are near 10% (a typical upper bound for relative errors).

Table 5
ERD_A Index evaluated using the approximated and exact models of the distribution network.

Case	ERD_A index (%)		Relative error (%)
	Exact model	Approximated model	
Without DG	27.6845	30.9573	11.8218
With conventional DG	88.9948	98.9054	11.1362

Table 6
Characteristics of PVDG.

Characteristic	Value
Rated power ($T = 25^\circ$ and $G = 1 kw/m^2$)	748.10 kW
Inverter power factor	0.9199
Number of modules in series by string	78
Number of strings in parallel	48
Occupied area	5281.8 m^2

4.2. Case studies analysis

The proposed methodology to estimate power PQI in distribution networks considering the presence of PVDG has been tested taking into account three case studies:

(i) Case #0 (base case): the test feeder without DG installation and considering only the load stochastic fluctuations.
(ii) Case #1: the test feeder with three PVDG installed in the nodes indicated in Fig. 4 and considering the uncertainties related to: load fluctuations, solar irradiance, temperature, and PVDG reliability. The reliability data of the PVDG were obtained from [25,28]. The main characteristics of the PVDG are presented in Table 6. It is assumed that the PVDG is composed of KC200GT PV modules. The electrical parameters of these modules were obtained from [23,24]. Usually, the PVDG is connected in the roof top of the customer's facilities, that is, the PVDG is dispersed within the low voltage distribution network and occupies a small area. In this paper, it is considered that the PVDG occupies a large area and is concentrated in a single load point. This trend is due to the fact that the local distribution utility is interested in assessing the impact of the "smart parking" on the PQI. That is, the parking of commercial buildings covered by photovoltaic arrays with the aim of selling electric energy.
(iii) Case #2: the test feeder with three conventional DG installed in the nodes specified in Fig. 4 and considering the uncertainties related to: load fluctuations and DG reliability. The main characteristics of the conventional DG are presented in Table 7. The DG reliability data were obtained from [29].

The PQI for all the case studies were evaluated considering a sample of one thousand weekly scenarios. Figs. 5 and 6 show the $IRD_{A,i}$, index based on the EN 50160, for the case studies #0 and #1, respectively. From these figures, it can be observed that the PVDG

Table 7
Characteristics of conventional DG.

Characteristic	Value
DG fuel	Natural gas
Rated active power	750 kW
Rated reactive power	319.4987 kVAr
Unavailability	4.6%

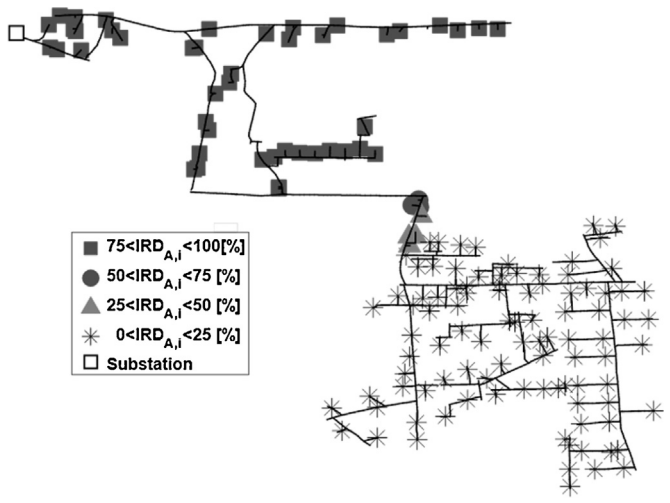

Fig. 5. GIS visualization of the $IRD_{A,I}$, index based on EN 50160 for the case study #0.

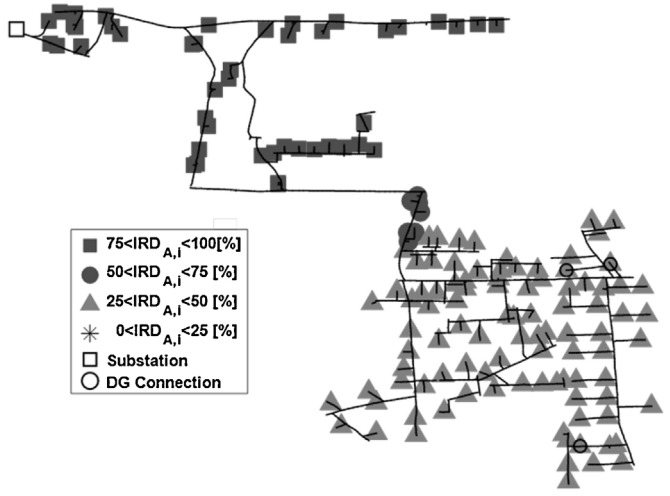

Fig. 6. GIS visualization of the $IRD_{A,I}$, index based on EN 50160 for the case study #0.

causes a significant improvement in the relative duration of the adequate state for the load points. For example, the PVDG connection eliminates all the $IRD_{A,i}$, indices lower than 25% (load points marked with asterisk). This result was expected for the reason that the DG connection decreases the feeder loading in the branches which in turn reduces the voltage drops. On the other hand, after connecting the conventional DG the $IRD_{C,I}$, index for all the loads was greater than 75%. This result is due to the conventional DG be operated continuously during the weekly period (base load operation model) while the PVDG cannot produce energy in periods without solar radiation (nighttime).

Table 8 presents the expected values of the systemic indices ERDA, ERDP, ERDC and CIC for the test feeder. This table shows the

Table 8
Expected values of the systemic indices.

Indices	Case #0	Case #1	Case #2	Variation (%)	
				Case #1	Case #2
ERD_A	27.55	36.207	87.08	31.42	216.07
ERD_P	57.44	50.96	12.87	−11.28	−77.59
ERD_C	15.00	12.83	0.0388	−14.46	−99.74
CIC	69.31	68.64	5.95	−0.9667	−91.41

Table 9
Risk of violating targets defined in EN 50160.

Risk interval (%)	Percentage of customers (%)		
	Case #0	Case #1	Case #2
0 ≤ risk < 25	8.5863	8.5863	25.6885
25 ≤ risk < 50	0.0000	0.0000	0.6384
50 ≤ risk < 75	0.0000	0.0000	29.7571
75 ≤ risk ≤ 100	91.4137	91.4137	43.9160

variations (in percentage) in the systemic indices for the cases #1 and #2 regarding to the case #0 (base case). From Table 8, it can be concluded that the DG insertion in the test feeder causes expressive improvements in the systemic voltage conformity indices. As well as in the nodal voltage conformity indices, the biggest improvements in the systemic voltage conformity indices were associated with the conventional DG (case #2). For example, the connection of the PVDG causes a reduction around 14.46% in the ERD_C, but the reduction in this index related to the conventional DG is near 99.74%.

Table 9 shows the percentage of customers associated with the risk of violating targets for voltage conformity indices based on EN 50160. From this table, it can be observed that the PVDG connection does not change the risk levels for the customers. In contrast, the connection of conventional DG contributes for a substantial reduction in the risk. Again, the explanation for this result is the DG operation mode: conventional DG is operated during all the time while the PVDG can produce energy only when there is sunlight.

Fig. 7 shows the voltage unbalance index for the test feeder. From this figure, it can be concluded that the DG insertion in the test feeder causes a reduction in the voltage unbalance. This effect is because the DG injects equilibrated currents into the network. It is interesting to notice that the voltage unbalance indices for the case studies #0 (without DG) and #1 (with PVDG installed) are almost the same during the nighttime. This result is caused due to the absence of solar irradiation during the nighttime. Consequently, the PVDG cannot produce energy and the system operates as if there was no DG.

It is important to assess the effects of the DG connection on the existing voltage control devices in the distribution networks. In this way, the systemic voltage conformity indices were evaluated considering the installation of a voltage regulator in the

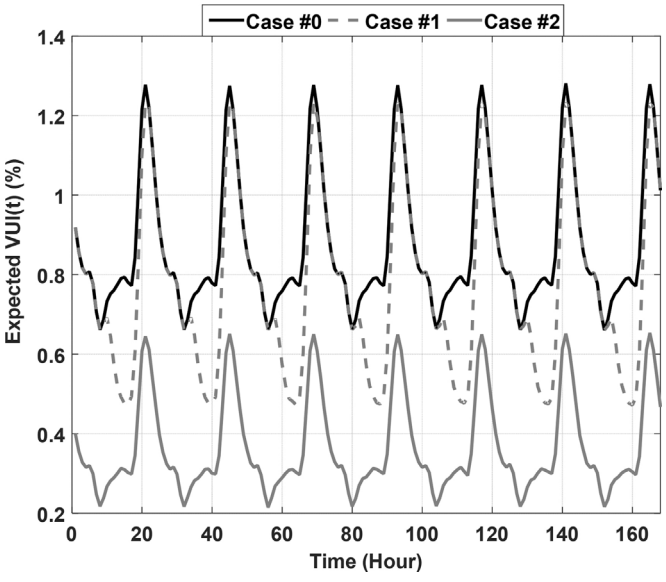

Fig. 7. Expected value of the voltage unbalance index.

Table 10
Systemic voltage conformity indices with voltage regulator.

Indices	Case #0	Case #1	Case #2	Variation (%)	
				Case #1	Case #2
ERD_A	91.55	76.65	87.72	−16.27	−4.18
ERD_P	7.74	22.95	12.28	196.51	58.65
ERD_C	0.71	0.40	0.00	−43.66	−100.00
CIC	13.96	9.19	0.00	−34.17	−100.00
Tap changes	138.60	110.33	5.51	−20.39	−96.02

substation node of the test feeder. The taps of this voltage regulator are adjusted to control the voltage magnitude in the node located in the center of the white circle with black border in Fig. 4. The controlled voltage node associated with the voltage regulator was determined using the state-invariant approach, based on the admittance matrix, proposed in [30]. The systemic voltage conformity indices associated with the voltage regulator for the three case studies are presented in Table 10. This table shows the expected number of tap changes per week for the case studies in the last row. Comparing the cases #0 of Tables 8 and 10, it can be noticed that the insertion of the voltage regulator caused significant improvements in the voltage conformity indices. For example, the increase in the ERD_A after installing the voltage regulator was near 232%. This result is coherent since the voltage regulator controls the nodal voltage magnitude in a node away from the substation. Consequently, the voltages in the nodes between the substation and the controlled voltage nodes are also improved due to the power flow in a passive distribution network be unidirectional. However, the addition of DG in the system with voltage regulator deteriorated the voltage conformity indices. For example, the increase in the equivalent relative duration of the non-adequate states ($ERD_P + ERD_C$) for the case study #1 was almost 176%. This effect is due to the DG had been installed near to the controlled voltage node. In this way, the voltage in the controlled voltage node is increased and the number of tap changes carried out by the voltage regulator to raise the voltage is decreased. For instance, the reduction in the number of tap changes in the case #2 is 96%. Therefore, the improvements in the voltages between the substation and the controlled voltage nodes are not as expressive as those achieved without DG. In other words, the DG installation masked the voltage conformity problems in the test feeder. The root cause of this problem is that substation voltage regulators are designed based on the principle that the voltage decreases from the substation node. This characteristic is lost when a DG is installed in a distribution network, since the voltages tend to increase in nodes near to the DG connection point. Therefore, more sophisticated techniques must be used to control var/volt in active distribution networks. On the other hand, there is a beneficial effect for the distribution utility in this scenario: the lifespan of the voltage regulator is increased since the number of tap changes required to carry out the voltage control is decreased. Fig. 8 shows the histogram of the number of tap changes for the three case studies. From this figure it can be noticed that the histograms for the case studies #1 and #2 (with DG connected) are closer to the vertical axis than the case #0 (without DG). In other words, the mean of the number of tap changes for the cases with DG is smaller than the one without DG. Fig. 8 shows that the insertion of DG in the test feeder causes a reduction in the number of tap changes.

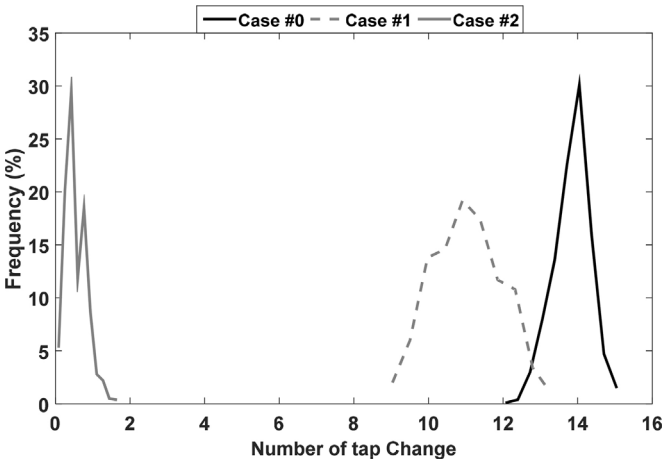

Fig. 8. Histogram of the number of tap changes for the case studies #0, #1 and #2.

5. Conclusions

This paper presents a probabilistic approach to evaluate PQI in distribution networks considering the presence of PVDG. The proposed approach is based on the combination of the following techniques: time series analysis, Quasi-Sequential Monte Carlo Simulation and radial power flow based on phase coordinates method. These three techniques were used to estimate the PQI related to voltage conformity and unbalance. The test results in a feeder with 1595 nodes demonstrate that:

(i) The voltage unbalance index undergoes large variations when the DG is connected to distribution networks;
(ii) The effect of PVDG on the PQI is lower than the one related to the conventional DG since the latter is operated continuously while the PVDG can produce energy only in sunshine period;
(iii) The voltage conformity indices are deteriorated when DG is added in a feeder with voltage regulator;
(iv) The connection of DG increases the lifespan of the voltage regulators due to the reduction on the number of tap changes.

References

[1] F.J. Ruiz-Rodriguez, J.C. Hernández, F. Jurado, Voltage unbalance assessment in secondary radial distribution networks with single-phase photovoltaic systems, Int. J. Electr. Power Energy Syst. 64 (2015) 646–654.
[2] F.J. Ruiz-Rodriguez, J.C. Hernandez, F. Jurado, Harmonic modelling of PV systems for probabilistic harmonic load flow studies, Int. J. Circuit Theory Appl. 43 (11) (2015) 1541–1565.
[3] J.C. Hernández, M.J. Ortega, A. Medina, Statistical characterisation of harmonic current emission for large photovoltaic plants, Int. Trans. Electr. Energy Syst. 24 (8) (2014) 1134–1150.
[4] ANEEL – Agência Nacional de Energia Elétrica, Procedimentos de Distribuição de Energia Elétrica no Sistema Elétrico Nacional – PRODIST, Módulo 8 – Qualidade da Energia Elétrica, ANEEL, 2011.
[5] EN 5016, Voltage Characteristics of Electricity Supplied by Public Distribution Systems, 1999.
[6] Y. Chen, J. Wen, S. Cheng, Probabilistic load flow method based on Nataf Transformation and Latin Hypercube Sampling, IEEE Trans. Sustain. Energy 4 (2) (2013) 294–301.
[7] F.J. Ruiz-Rodriguez, J.C. Hernández, F. Jurado, Probabilistic load flow for photovoltaic distributed generation using the Cornish–Fisher expansion, Electr. Power Syst. Res. 89 (2012) 129–138.
[8] F. Vallée, V. Klonari, T. Lisiecki, O. Durieux, F. Moiny, J. Lobry, Development of a probabilistic tool using Monte Carlo simulation and smart meters measurements for the long term analysis of low voltage distribution grids with photovoltaic generation, Int. J. Electr. Power Energy Syst. 53 (2013) 468–477.
[9] A. Bracale, P. Caramia, G. Carpinelli, A.R. Di Fazio, P. Varilone, A Bayesian-based approach for a short-term steady-state forecast of a smart grid, IEEE Trans. Smart Grid 4 (4) (2013) 1760–1771.
[10] J.C. Hernández, F.J. Ruiz-Rodriguez, F. Jurado, Technical impact of photovoltaic-distributed generation on radial distribution systems: stochastic simulations for a feeder in Spain, Int. J. Electr. Power Energy Syst. 50 (2013) 25–32.
[11] A. Woyte, V.V. Thong, R. Belmans, J. Nijs, Voltage fluctuations on distribution level introduced by photovoltaic systems, IEEE Trans. Energy Convers. 21 (1) (2006) 202–209.
[12] J.M. Sexauer, S. Mohagheghi, Voltage quality assessment in a distribution system with distributed generation – a probabilistic load flow approach, IEEE Trans. Power Deliv. 28 (3) (2013) 1652–1662.
[13] J. Faiz, B. Siahkolah, Electronic Tap-changer for Distribution Transformers, Springer-Verlag, New York, 2011.
[14] F. Katiraei, J.R. Agüero, Solar PV integration challenges, IEEE Power Energy Mag. (2011, May/June) 62–71.

[15] J. Smith, M. Rylander, L. Rogers, R. Dugan, It's all in the plans: maximizing the benefits and minimizing the impacts of DERs in an integrated grid, IEEE Power Energy Mag. (2015, March/April) 20–29.
[16] F. Katiraei, C. Sun, B. Enayati, No inverter left behind: protection, controls, and testing for high penetrations of PV inverters on distribution systems, IEEE Power Energy Mag. (2015, March/April) 43–49.
[17] A.M. Leite da Silva, R.A. Gonzalez-Fernandez, W.S. Sales, L.A.F. Manso, Reliability assessment of time-dependent systems via quasi-sequential Monte Carlo Simulation, in: 2010 IEEE 11th International Conference on Probabilistic Methods Applied to Power Systems, 2010, pp. 697–702.
[18] W.H. Kersting, Distribution Systems Modeling and Analysis, CRC Press, Boca Raton, 2007.
[19] A.C. Silva, A.B. Rodrigues, M.G. Silva, Probabilistic evaluation of long-duration voltage variations in distribution networks with wind power plants, IET Gener. Transm. Distrib. 9 (13) (2015) 1526–1533.
[20] S.A. Soliman, A.M. Al-Kandari, Electrical Load Forecasting: Modeling and Model Construction, Elsevier/Butterworth-Heinemann, Burlington, 2010.
[21] M.J.E. Alam, K.M. Muttaqi, D. Sutanto, A three-phase power flow approach for integrated 3-wire MV and 4 – wire multigrounded LV networks with rooftop solar PV, IEEE Trans. Power Syst. 28 (2) (2013) 1728–1737.
[22] G.M. Masters, Renewable and Efficient Electric Power Systems, Wiley, Hoboken, 2004, pp. 527 (Chapter 9).
[23] M.G. Villalva, J.R. Gazoli, E. Ruppert, Filho, Comprehensive approach to modeling and simulation of photovoltaic arrays, IEEE Trans. Power Electron. 24 (5) (2009) 1198–1208.
[24] M.G. Villalva, Three-Phase Power Electronic Converter for Grid Connected Photovoltaic System (PhD Thesis), UNICAMP, 2010.
[25] P. Zhang, Y. Wang, W. Xiao, W. Li, Reliability evaluation of grid-connected photovoltaic power systems, IEEE Trans. Sustain. Energy 3 (3) (2012) 379–389.
[26] I.E.C. 61000-4-30, Electromagnetic Compatibility (EMC) – Part 4-30 Environment – Testing and Measurement Techniques – Power Quality Measurement Methods, International Eletrotechnical Commission, 2003.
[27] Power System Group of the Federal University of Maranhão (UFMA). "Reliability optimization in electric energy distribution networks", Research & Development Project – Companhia Energética do Maranhão (CEMAR), Final Report, January 2002–December 2002 (in Portuguese).
[28] S.V. Dhople, A.D. Domínguez-García, Estimation of photovoltaic system reliability and performance metrics, IEEE Trans. Power Electron. 27 (1) (2012) 554–563.
[29] H.L. Willis, W.G. Scott, Distributed Power Generation: Planning and Evaluation, CRC Press, Boca Raton, 2000.
[30] A.Z. Gamm, I.I. Golub, A. Bachry, Z.A. Styczynski, Solving several problems of power systems using spectral and singular analyses, IEEE Trans. Power Syst. 20 (1) (2005) 138–148.